Resolving the effects of production-induced overburden dilation using simultaneous TV-regularized time-lapse FWI

Musa Maharramov, Biondo Biondi and Mark Meadows

ABSTRACT

We present a field data application of the technique proposed by Maharramov and Biondi (2015) for reconstructing production-induced subsurface model changes from time-lapse seismic data using full-waveform inversion (FWI). The technique simultaneously inverts multiple survey vintages with total-variation (TV) regularization of the model differences. We apply it to the Gulf of Mexico, Genesis Field data, and successfully resolve negative velocity changes associated with overburden dilation and demonstrate that the results are stable with respect to the amount of regularization and consistent with earlier estimates of time strain in the overburden.

INTRODUCTION

Prevalent practice in time-lapse seismic processing relies on picking time displacements and changes in reflectivity amplitudes between migrated baseline and monitor images, and converting them into impedance changes and subsurface deformation (Johnston, 2013). This approach requires a significant amount of manual interpretation and quality control. One alternative approach uses the high-resolution power of full-waveform inversion (Sirgue et al., 2010a) to reconstruct production-induced changes from wide-offset seismic acquisitions (Routh et al., 2012; Zheng et al., 2011; Asnaashari et al., 2012; Raknes et al., 2013; Maharramov and Biondi, 2014a; Yang et al., 2014). However, while potentially reducing the amount of manual interpretation, time-lapse FWI is sensitive to repeatability issues (Asnaashari et al., 2012), with both coherent and incoherent noise potentially masking important production-induced changes. The joint time-lapse FWI proposed by Maharramov and Biondi (2013, 2014a) addressed repeatability issues by joint inversion of multiple vintages with model-difference regularization based on the L_2-norm and produced improved results when compared to the conventional time-lapse FWI techniques. Maharramov and Biondi (2015) extended this joint inversion approach to include edge-preserving total-variation (TV) model-difference regularization. The new method was shown to achieve a dramatic improvement over alternative techniques by significantly reducing oscillatory artifacts in the recovered model difference for synthetic data with

repeatability issues. In this work, we apply this TV-regularized simultaneous inversion technique to the Gulf of Mexico, Genesis Field data and demonstrate a stable recovery of production-induced model changes.

FWI applications in time-lapse problems seek to recover induced changes in the subsurface model by using multiple seismic datasets from different acquisition vintages. For two surveys sufficiently separated in time, we call such datasets (and the associated models) "baseline" and "monitor". Time-lapse FWI can be conducted by separately inverting the baseline and monitor models ("parallel difference", Plessix et al. (2010)) or inverting them sequentially with, e.g., the baseline supplied as a starting model for the monitor inversion ("sequential difference"). The latter may achieve a better recovery of model differences in the presence of incoherent noise (Asnaashari et al., 2012; Maharramov and Biondi, 2014a). Another alternative is to apply the "double-difference" method (Watanabe et al., 2004; Denli and Huang, 2009; Zheng et al., 2011; Asnaashari et al., 2012; Raknes et al., 2013). The latter approach may require significant data pre-processing and equalization (Asnaashari et al., 2012; Maharramov and Biondi, 2014a) across survey vintages. In all of these techniques,

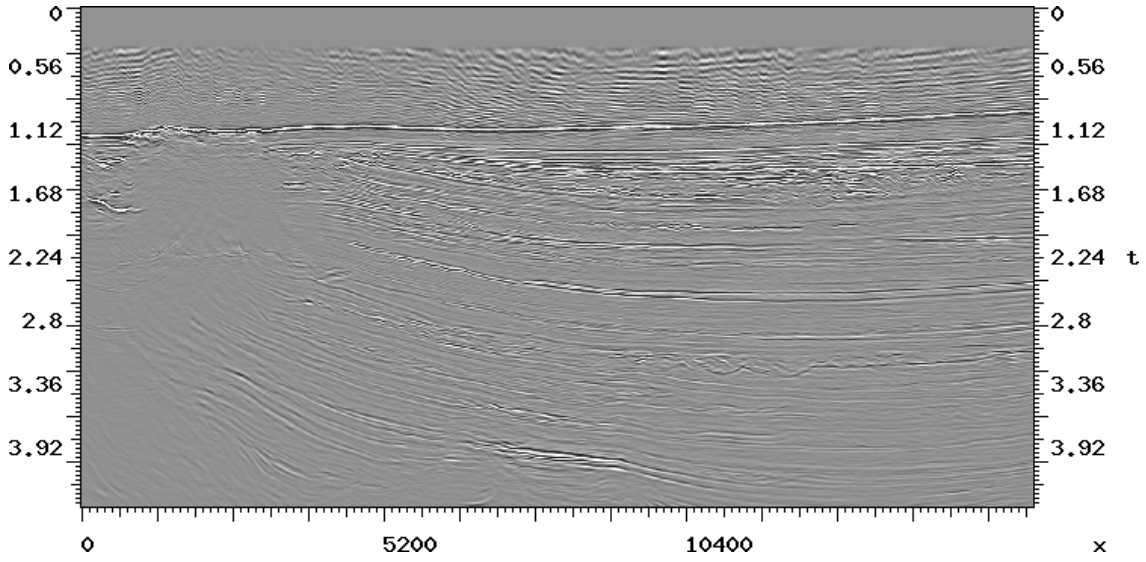

Figure 1: A north-south inline section of the baseline Genesis image produced by Chevron (vertical axis two-way travel time in seconds, horizontal axis inline meters). [**NR**]

optimization is conducted with respect to one model at a time, albeit of different vintages at different stages of the inversion.

METHOD

We propose to invert the baseline and monitor models simultaneously by solving the following optimization problem (Maharramov and Biondi, 2015):

$$\alpha\|\mathbf{u}_b(\mathbf{m}_b)-\mathbf{d}_b\|_2^2+\beta\|\mathbf{u}_m(\mathbf{m}_m)-\mathbf{d}_m\|_2^2+ \tag{1}$$

$$\delta\|\mathbf{WR}(\mathbf{m}_m-\mathbf{m}_b)\|_1 \;\rightarrow\; \min \tag{2}$$

with respect to both the baseline and monitor models $\mathbf{m}_b$ and $\mathbf{m}_m$. Problem (1,2) describes time-lapse FWI with the L_1 regularization of the transformed model difference (2). The terms (1) correspond to separate baseline and monitor inversions with observed data $\mathbf{d}$ and modeled data $\mathbf{u}$. In (2), $\mathbf{R}$ and $\mathbf{W}$ denote regularization and weighting operators, respectively. If $\mathbf{R}$ is the gradient magnitude operator

$$\mathbf{R}f(x,y,z) \;=\; \sqrt{f_x^2+f_y^2+f_z^2}, \tag{3}$$

then (2) becomes the "Total Variation" (TV) seminorm. This case is of particular interest, because minimization of the gradient L_1 norm promotes "blockiness" of the model-difference, potentially reducing oscillatory artifacts (Rudin et al., 1992). Total-variation regularization, known in image processing as the "ROF Model", was applied earlier to full-waveform inversion as a way of resolving sharp geologic boundaries (Anagaw and Sacchi, 2012). The solution of a large-scale optimization problem based on the ROF model using conventional methods is computationally challenging, prone to the "staircasing effect" (Chambolle and Lions, 1997), and may require solution methods that involve splitting and gradient thresholding (Goldstein and Osher, 2009). However, time-lapse FWI appears to be a nearly ideal application for the ROF model, because significant production-induced subsurface model changes are spatially bounded and have magnitudes that can be roughly estimated *a priori* from geomechanical and production data (Maharramov and Biondi (2014a), supplementary material). More specifically, the weighting operator $\mathbf{W}$ may be obtained from prior geomechanical information. For example, a rough estimate of production-induced velocity changes can be obtained from time shifts (Hatchell and Bourne, 2005) and used to map subsurface regions of expected production-induced perturbation.

APPLICATION TO FIELD DATA

The Genesis Field, operated by Chevron, is located 150 miles southwest of New Orleans in the Green Canyon area of the central Gulf of Mexico, in approximately 770-830m of water (Magesan et al., 2005). Oil was found in several late Pliocene through early Pleistocene deep-water reservoirs. Most of the field's oil and gas reserves are in the early Pleistocene Neb 1, Neb 2, and Neb 3 reservoirs that are the primary subject of this study. First oil production began in January 1999.

A 3D seismic survey was shot in 1990, and a time-lapse survey was shot in October 2002 with the aim of improving field management (Hudson et al., 2005; Magesan et al.,

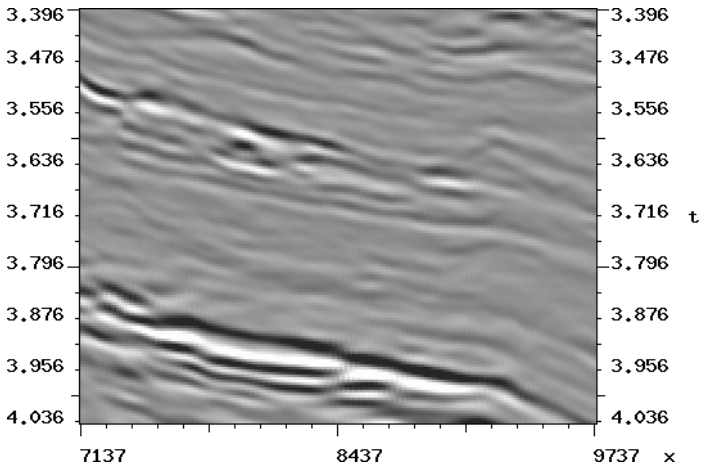

Figure 2: Monitor and baseline image-difference obtained from the 3D time-migration images provided by Chevron which corresponds to the inline section of Figure 1. Production-induced changes stand out at approximately 3.5 s (wet Illinoisan sands) and 4 s two-way travel times—stacked Neb 1, 2, and 3 reservoirs—compare with Hudson et al. (2005). [**NR**]

2005). Cumulative production from the field at the time of the monitor survey was more than 57 MMBO, 89 MMCFG, and 19 MMBW (Hudson et al., 2005).

In addition to fluid substitution effects, producing reservoirs compact, increasing the depth to the top of the reservoirs and causing overburden dilation (Johnston, 2013). A time-lapse study performed by Chevron (Hudson et al., 2005) indicated significant apparent kinematic differences in the Pleistocene reservoir interval. Time shifts were observed both for the producing reservoirs and Illinoisan wet sands above Neb 1 (see Figure 3). Kinematic differences were attributed to a time shift caused by subsidence at the top of the uppermost reservoir, subsidence of the overburden, and overburden dilation (Hudson et al., 2005).

Processing parameters for the baseline and monitor surveys and subsequent time-lapse processing by Chevron were described by Magesan et al. (2005). The baseline survey had a maximum offset of 5 km, and the monitor survey had a maximum offset of 7.3 km. Both surveys used a bin size of 12.5 m by 37 m. For the purpose of time-lapse analysis, the acquired data had been subjected to pre-processing and imaging steps that included data equalization, spherical divergence correction, source and receiver statics, global phase rotation, time shift, amplitude scaling, global spectral matching, and cross-equalization (Magesan et al., 2005).

The data pre-processed for time-lapse analysis were used by Chevron in Kirchhoff time migration of the baseline and monitor surveys, producing 3D images. A single inline section of the baseline image is shown in Figure 1. The corresponding monitor and baseline image difference is shown in Figure 2. As noted by Hudson et al. (2005), the image difference is contributed to by time shifts at the Illinoisan sands (upper

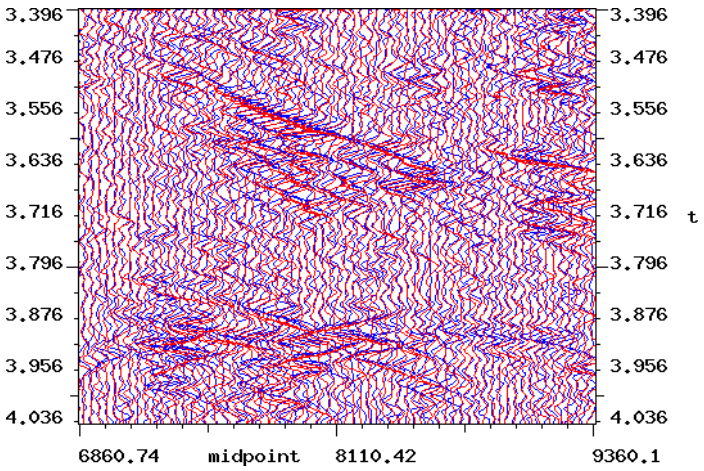

Figure 3: Production-induced changes resulted in measurable time-shifts between the surveys. Shown here are time-shifts between the baseline (blue) and monitor (red) common-offset gathers, 1074 m offset. [**CR**]

event) and Neb 1 (lower event) in Figure 2—compare with Figure 1 of Hudson et al. (2005).

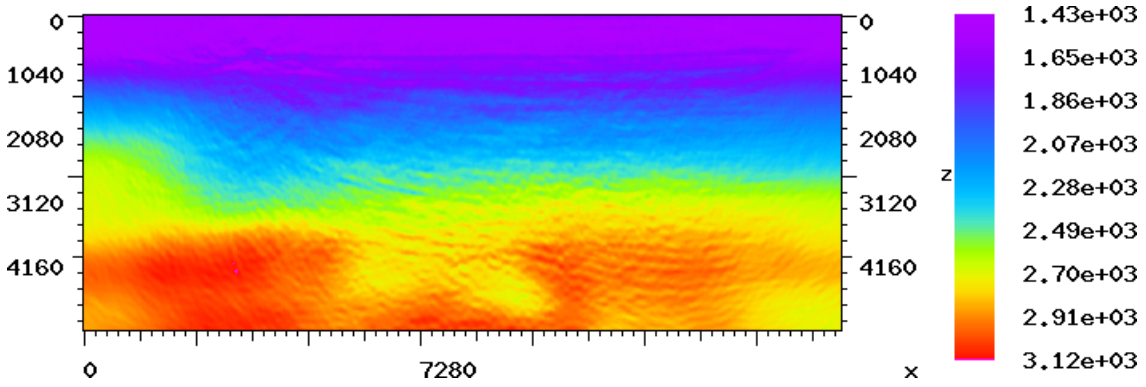

Figure 4: Inverted baseline velocity model. FWI resolved fine model features and oriented them along the dip structure of the image in Figure 1 (vertical axis depth meters). [**CR**]

The purpose of this application was to see whether or not joint regularized time-lapse FWI could resolve some of the production-induced model differences, thus providing additional insight into reservoir depletion patterns and optimal infill drilling strategies. As our first processing step, we performed separate baseline and monitor 2D full-waveform inversion of a single inline section. We extracted a single north-south inline corresponding to the image in Figure 1 from both surveys and sorted it into shot gathers with a minimum offset of 350 m and a maximum offset of 4,700 m. This provided 1,264 shots with up to 175 receivers per shot. A frequency-domain 2D FWI (Sirgue et al., 2008, 2010b) was conducted over the frequency range of 3-30.7 Hz. Frequency spacings were selected using the technique of Sirgue and Pratt (2004).

The data provided to us had undergone amplitude pre-processing that included a spherical divergence correction. Furthermore, accurate handling of the amplitudes in 2D FWI of 3D field data requires a 3D-to-2D data transformation (Auer et al., 2013). Because the data exhibited significant time-shifts at the reservoir level (Hudson et al., 2005) that can be readily observed even at far offsets (see Figure 3), we decided to use a "phase-only" inversion and ignored amplitude information in the data (Fichtner, 2011).

The result of baseline inversion is shown in Figure 4. To build a starting model for the FWI, we converted Chevron's RMS time-migration velocity model to an interval velocity using the Dix equation, and smoothed the result using a triangular filter with a 41-sample window. Observe that FWI succeeded in resolving fine features, and oriented them consistently along the dip structure of the time-migrated image in Figure 1. Close-up views of the model area covering both the Illinoisan sands and the reservoirs are shown in Figures 6(a) and 6(c).

The result of parallel differencing is shown in Figure 5(a). Although significant model changes appear to be concentrated around the target area, this result is not interpretable, either qualitatively or quantitatively, because it is contaminated with oscillatory artifacts and overestimates the magnitudes of velocity perturbations. This result is consistent with our earlier assessment of conventional time-lapse FWI techniques tested on synthetic data (Maharramov and Biondi, 2014a, 2015).

Next, we solved the simultaneous, TV-regularized time-lapse full-waveform inversion problem (1,2). We set $\alpha = \beta = 1$ and carried out multiple experiments with the value of the regularization parameter δ ranging from $\delta = 100$ to $\delta = 1000$. The weighting operator $\mathbf{W}$ was set to 1 inside the larger target area shown in Figures 5(a) through 6(b), and tapered off to zero outside.

The results of inverting the model difference for $\delta = 100$, 500 and 1000 are shown in Figures 5(b), 5(c), and 5(d), respectively. Gradual increase of the regularization parameter results in the removal of most model differences with the exception of a negative velocity perturbation in the overburden, peaking at approximately 3.6 km and 3.9 km (see Figures 6(b) and 6(d)). Such perturbations are consistent with overburden dilation due to the compaction of stacked reservoirs, with more significant dilation in the wet Illinoisan sands than the surrounding shales (Rickett et al., 2007). The zone of negative velocity change appears to extend upward into the overburden in a direction roughly orthogonal to the reservoir dip—see Figure 5(d). Two negative velocity changes at approximately 10 and 11.5 km inline persist with increasing regularization, and may represent dilation effects associated with the production from deeper reservoirs—compare with Figure 3 of Rickett et al. (2007).

The estimated maximum negative velocity change of -45 m/s above the stacked reservoirs is consistent with the earlier estimates of time strain in the overburden (Rickett et al., 2007). Indeed, local time strain, physical strain and partial velocity

change are related by the equation (Hatchell and Bourne, 2005)

$$\frac{d\tau}{dt} \approx \frac{\Delta t}{t} = \frac{\Delta z}{z} - \frac{\Delta v}{v}, \tag{4}$$

where τ, t, z, and v denote the observed time shift, travel time, depth, and velocity. Assuming, following Hatchell and Bourne (2005), that

$$\frac{\Delta v}{v} = -R\frac{\Delta z}{z}, \tag{5}$$

where the factor R is estimated to be 6 ± 2 for the Genesis overburden (Hodgson et al., 2007), we obtain

$$\frac{\Delta v}{v} = -\frac{R}{R+1}\frac{\Delta t}{t} \approx -\frac{\Delta t}{t} \approx -\frac{d\tau}{dt}. \tag{6}$$

Maximum time strains in the Genesis overburden are estimated to be around +2% (Rickett et al., 2007), yielding the maximum negative velocity change of

$$\Delta v \approx -.02 \times 2,800 \text{ m/s} = -56 \text{ m/s}, \tag{7}$$

where the estimated P-wave velocity of 2,800 m/s at a 3.6 km depth was taken from the output of our FWI.

CONCLUSIONS

Simultaneous time-lapse FWI with total-variation difference regularization can achieve robust recovery of production-induced changes, preserving the blocky nature of monitor-baseline differences. Velocity changes caused by overburden dilation are within the resolution of our method. However, velocity changes within thin reservoirs (e.g., caused by compaction) can no longer be characterized as "blocky" on a seismic scale, and recovering such changes may require a multi-norm model decomposition approach *a la* Maharramov and Biondi (2014b), and will be the subject of further research.

ACKNOWLEDGMENTS

The authors would like to thank the affiliate members of Stanford Exploration Project (SEP) for their support; Joseph Stefani, Stewart Levin, Shuki Ronen, and Dimitri Bevc for a number of useful discussions; Chevron, ExxonMobil, and BHP Billiton for providing the field data; and the Stanford Center for Computational Earth and Environmental Science for providing computing resources.

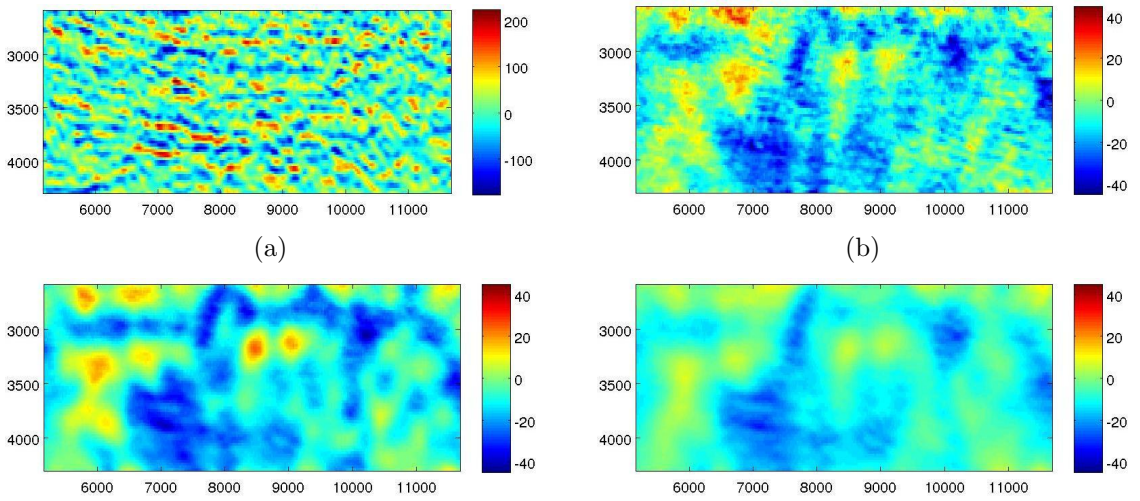

Figure 5: (a) Parallel difference and joint inversion results for (b) $\delta = 100$, (c) $\delta = 500$, and (d) $\delta = 1000$ in the target area. The parallel difference result is not interpretable because of the presence of artifacts. Increasing the regularization parameter δ results in gradual removal of most model differences except the negative velocity change in the overburden, peaking around the Illinoisan sands and near the top of the stacked reservoirs—see Figures 6(a) through 6(d). [**CR**]

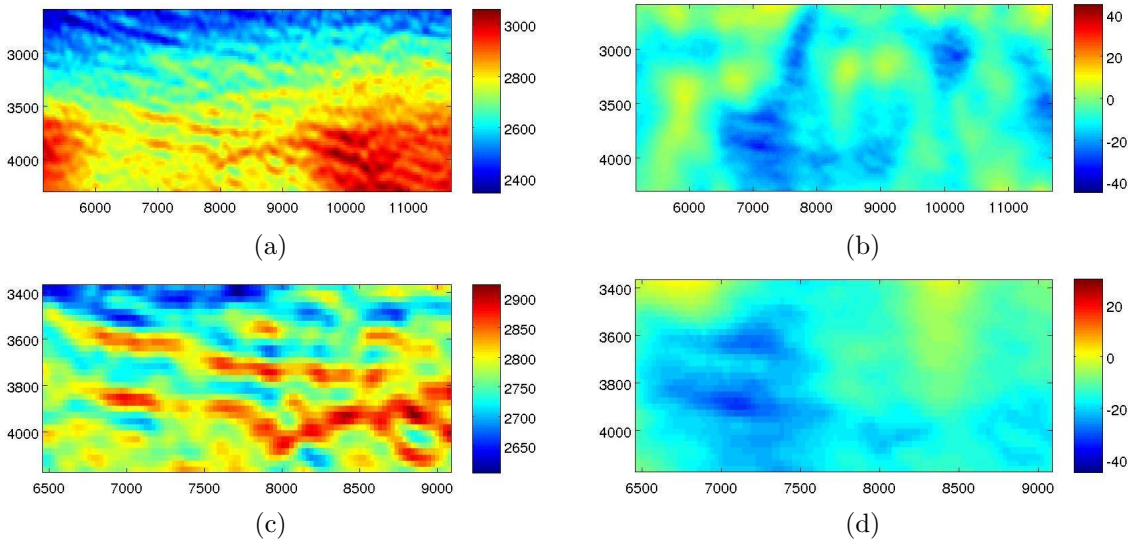

Figure 6: (a) Baseline target area and (b) estimated model difference for $\delta = 1000$. Close-up of (c) baseline target area and (b) estimated model difference for $\delta = 1000$. [**CR**]

REFERENCES

Anagaw, A. Y. and M. D. Sacchi, 2012, Edge-preserving seismic imaging using the total variation method: Journal of Geophysics and Engineering, **9**, 138.

Asnaashari, A., R. Brossier, S. Garambois, F. Audebert, P. Thore, and J. Virieux, 2012, Time-lapse imaging using regularized FWI: A robustness study: 82nd Annual International Meeting, SEG, Expanded Abstracts, doi:10.1190/segam2012-0699.1, 1–5.

Auer, L., A. M. Nuber, S. A. Greenhalgh, H. Maurer, and S. Marelli, 2013, A critical appraisal of asymptotic 3D-to-2D data transformation in full-waveform seismic crosshole tomography: Geophysics, **78**, no. 6, R235–R247.

Chambolle, A. and P. L. Lions, 1997, Image recovery via total variational minimization and related problems: Numerische Mathematik, **76**, 167–188.

Denli, H. and L. Huang, 2009, Double-difference elastic waveform tomography in the time domain: 79th Annual International Meeting, SEG, Expanded Abstracts, 2302–2306.

Fichtner, A., 2011, Full seismic modeling and inversion: Springer.

Goldstein, T. and S. Osher, 2009, The split Bregman method for L1-regularized problems: SIAM Journal on Imaging Sciences, **2**, 323–343.

Hatchell, P. and S. Bourne, 2005, Measuring reservoir compaction using time-lapse timeshifts: 75th Annual International Meeting, SEG, Expanded Abstracts, 2500–2503.

Hodgson, N., C. Macbeth, L. Duranti, J. Rickett, and K. Nihei, 2007, Inverting for reservoir pressure change using time-lapse time strain: Application to Genesis Field, Gulf of Mexico: The Leading Edge, **26**, 649–652.

Hudson, T., B. Regel, J. Bretches, J. Rickett, B. Cerney, and P. Inderwiesen, 2005, Genesis Field, Gulf of Mexico, 4D project status and preliminary lookback: 75th Annual International Meeting, SEG, Expanded Abstracts, 2436–2439.

Johnston, D., 2013, Practical applications of time-lapse seismic data: Society of Exploration Geophysicists.

Magesan, M., S. Depagne, K. Nixon, B. Regel, J. Opich, G. Rogers, and T. Hudson, 2005, Seismic processing for time-lapse study: Genesis Field, Gulf of Mexico: The Leading Edge, **24**, 364–373.

Maharramov, M. and B. Biondi, 2013, Simultaneous time-lapse full waveform inversion: SEP Report, **150**, 63–70.

———, 2014a, Joint full-waveform inversion of time-lapse seismic data sets: 84th Annual Meeting, SEG, Expanded Abstracts, 954–959.

———, 2014b, Multi-model full-waveform inversion: SEP Report, **155**, 187–192.

———, 2015, Robust simultaneous time-lapse full-waveform inversion with total-variation regularization of model difference: 77th EAGE Conference and Exhibition, Extended Abstracts (accepted).

Plessix, R.-E., S. Michelet, H. Rynja, H. Kuehl, C. Perkins, J. W. de Maag, and P. Hatchell, 2010, Some 3D applications of full waveform inversion: 72nd EAGE Conference and Exhibition, Workshop WS6 "3D Full Waveform Inversion—A Game Changing Technique?".

Raknes, E., W. Weibull, and B. Arntsen, 2013, Time-lapse full waveform inversion: Synthetic and real data examples: 83rd Annual International Meeting, SEG, Expanded Abstracts, 944–948.

Rickett, J., L. Duranti, T. Hudson, B. Regel, and N. Hodgson, 2007, 4D time strain and the seismic signature of geomechanical compaction at Genesis: The Leading Edge, **26**, 644–647.

Routh, P., G. Palacharla, I. Chikichev, and S. Lazaratos, 2012, Full wavefield inversion of time-lapse data for improved imaging and reservoir characterization: 82nd Annual International Meeting, SEG, Expanded Abstracts, doi:10.1190/segam2012-1043.1, 1–6.

Rudin, L. I., S. Osher, and E. Fatemi, 1992, Nonlinear total variation based noise removal algorithms: Physica D: Nonlinear Phenomena, **60**, 259–268.

Sirgue, L., O. Barkved, J. Dellinger, J. Etgen, U. Albertin, and J. Kommendal, 2010a, Full waveform inversion: The next leap forward in imaging at Valhall: First Break, **28**, no. 4, 65–70.

Sirgue, L., J. T. Etgen, and U. Albertin, 2008, 3D frequency domain waveform inversion using time domain finite difference methods: 70th EAGE Conference and Exhibition, Extended Abstract, F022.

Sirgue, L., J. T. Etgen, U. Albertin, and S. Brandsberg-Dahl, 2010b, System and method for 3D frequency domain waveform inversion based on 3D time-domain forward modeling. (US Patent 7,725,266).

Sirgue, L. and R. Pratt, 2004, Efficient waveform inversion and imaging: A strategy for selecting temporal frequencies: Geophysics, **69**, 231–248.

Watanabe, T., S. Shimizu, E. Asakawa, and T. Matsuoka, 2004, Differential waveform tomography for time-lapse crosswell seismic data with application to gas hydrate production monitoring: 74th Annual International Meeting, SEG, Expanded Abstracts, 2323–2326.

Yang, D., A. E. Malcolm, and M. C. Fehler, 2014, Time-lapse full waveform inversion and uncertainty analysis with different survey geometries: 76th EAGE Conference and Exhibition, Extended Abstract, We ELI1 10.

Zheng, Y., P. Barton, and S. Singh, 2011, Strategies for elastic full waveform inversion of timelapse ocean bottom cable (OBC) seismic data: 81st Annual International Meeting, SEG, Expanded Abstracts, 4195–4200.